Chapter 12
Spatial Pattern Analysis and Identifying Soil Pollution Hotspots Using Local Moran's I and GIS at a Regional Scale in Northeast of Iran

Ali Keshavarzi, Gouri Sankar Bhunia, Pravat Kumar Shit, Güneş Ertunç, and Mojtaba Zeraatpisheh

Abstract The spatial distribution of soil physicochemical characteristics and four heavy metals (Mn, Fe, Zn, and Cu) in the semi-arid climatic region of Neyshabur plain in Northeast of Iran was investigated and identified soil pollution hotspots zone using Moran's I and GIS techniques. The geostatistical techniques, Pearson's correlation matrix, and spatial autocorrelation were used to locate the pollution sources and concentration. Geostatistical interpolation techniques determined the spatial distribution of heavy metals. The mean values of Iron (Fe), Manganese (Mn), Zink (Zn), Copper (Cu) were 2.31, 7.18, 2.84, 1.16 mg/kg, respectively. The routs comes of the spatial statistical method have established the gravity of pollutions and their anthropogenic impact based on spatial changes in contamination levels. The genesis of the pollution process was influenced by natural factors (e.g., the high soil shale, the sandstone, the calcareous and the metamorphic parents and the background values) as well as by anthropogenic factors (e.g., waste disposal, extraction from mines of distinct mineral ores and high, unmanaged practices of fertilizer). Although nearly

A. Keshavarzi (✉)
Laboratory of Remote Sensing and GIS, Department of Soil Science, University of Tehran, P.O.Box: 4111, 31587-77871 Karaj, Iran
e-mail: alikeshavarzi@ut.ac.ir

G. S. Bhunia
Paschim Medinipur, Kharagpur, West Bengal 721424, India

P. K. Shit
Department of Geography, Raja NL Khan Women's College, Gope Palace, Medinipur, West Bengal 721102, India

G. Ertunç
Department of Mining Engineering, Hacettepe University, 06800 Beytepe, Ankara, Turkey
e-mail: gertunc@hacettepe.edu.tr

M. Zeraatpisheh
Henan Key Laboratory of Earth System Observation and Modeling, Henan University, Kaifeng 475004, China

College of Geography and Environmental Science, Henan University, Kaifeng 475004, China

all the monitoring classes of land use suffered from contamination by heavy metals, farmland was the most contaminated. This evidence will help land use planners and environmental menace administrators to promote environmentally sound economic expansion policies.

Keywords Environmental pollution · Geostatistics · GIS · Heavy metals · Hotspots zone · Iran

12.1 Introduction

The natural components of the earth's crust are heavy metals. A number of these constituents are of biological importance and play an important part in human life when they trace the water, the air, dust, soils, and sediments. The soil is the most polluting habitat as a "universal trap." In a variety of cases, it gets tainted. Okrent (1999) stated that soil pollution is demarcated as the growth of obstinate toxic soils, chemicals, salt, or disease-causing substances that adversely affect crop growth and animal health. Soil pollution must be monitored urgently to protect soil fertility and increase productivity. One main source of heavy metals in the soil, and is accountable for an improved pervasiveness and incidence of heavy metal pollution on the Earth's surface, is anthropogenic activity such as mining and metal smelting (Bhattacharya et al. 2006). Generally, water, sewage, improper dumping or by-products, or contamination from the processing of something of value absorbs much of the pollutants into the ecosystem (Soffianian et al. 2014). Opencast mining operations, which produced millions of tons of sulfide-rich waste, have a significant environmental effect on soils and water sources (Parizanganeh et al. 2010). By accelerating erosion, we somewhat lose this important natural resource. Besides that, the enormity of man-made waste, sludge, and other products' from new waste treatment plants also cause or lead to polluted soil. To sustain the fertility and productivity of the soil, rigorous control measures must be implemented, hence increasing the health of all living things.

Evaluating the ecological menace of polluted soil, pesticide application, sewage sludge, and other anthropogenic activities resulting in exposure to hazardous substances in the terrestrial environment is a complex task with manyalliedglitches. In the present way that we evaluate the menace and the effect of anthropogenic agents on the terrestrial climate, even though those factors were ignored, there are a variety of unanswered issues. An assessment of the bioavailable percentage of radioactive metals may be carried out to assess soil contamination of heavy metals. Soil metal mobility has commonly been evaluated by a chemical method based on selective withdrawals.

Iran has experienced broad developments in the last four decades, including rapid urbanization, industrial development, and intensive cultivation in many regions. Sometimes these variations have been escorted by neglected environmental devaluation (Moghtaderi et al. 2018, 2019; Khamesi et al. 2020). This is also an imperative zone for agriculture where crops like maize, barley, and sugar beet are grown. Soils

can be polluted by industrial and urban contaminations in agricultural areas, posing a danger to humans, as showed by Doabi et al. (2018, 2019) in other areas of Iran, by consuming food grown in these countries.

Geospatial analytical techniques are key tools for soil parameter characterization (Hou et al. 2017). In previous soil pollution studies, classical statistical methods have been commonly used, but these approaches are affluent and time-consuming and do not quantify assessment errors. Soil contamination can be well known by Geographic Information System (GIS) and geostatistical methods at present (Soffianian et al. 2015). In order to assess the spatial structure of heavy metals and soil physico chemical characteristics, GIS are essential for the implementation through geostatistical and multivariate analyses (Santos-Francés et al. 2017). In fact, it is not possible to arrange adequate samples from the subject areas. Therefore, spatial statistical approaches haves wapped traditional statistics, as they can precisely detect pollutant changes in time and space and calculate estimation errors (Soffianian et al. 2014). Several studies have examined spatial distribution in industrial areas worldwide of heavy metal pollution in the surface ground. For instance, Wang et al. (2017) reported a less national standard but less than the natural baseline values for the geographical dispersal of Cu, Zn, Cr, Cd, As, and Hg concentrations in the industrial area of Sichuan, China. In the industrial city of Aran-o-Bidgol, Iran, Ravankhah et al. (2016) carried out the assessment of the ecological menace of heavy metals from surface soil. The Cd, Pb, Ni, and Cu levels were recorded above the background values.

The study was showed in order to classify the area where heavy metals are tainted. More specifically, first the spatial distribution of some main soil properties and heavy metals such as pH, OC, Sand, Silt, Clay, Phosphorus, Fe, Mn, Zn, and Cu were determnined and then the spatial distribution of soil properties and heavy metals were applied to find toxic hotspots and to detect potential causes of contaminants in surface soils in the Neyshabur plain, Khorasan-e-Razavi Province, Northeast Iran. Moreover, in order to reduce the uncertainties associated with parameters, the datasets were further statistically analyzed using statistical approaches such as the correlation matrix, spatial autocorrelation, and spatial modeling.

12.2   Study Area

The research was carried out in a catchment in the part of Neyshabur plain of Khorasan-e-Razavi Province (36°2′–36°10′ N, and 58°52′–59°07′ E) of Northeast Iran (Fig. 12.1). The study area covers by an area of almost 170 km^2 with an elevation of 1256 m above mean sea level. The region is considered by the semi-arid climate with mean temperature of 14.5 °C and annual precipitation of 233.7 mm. The primary land use structure of the area is irrigated farming (Bagherzadeh et al. 2016). The general slope of the plain extends in NW–SE direction. The major land type is described as piedmont plain and Qft2 unit is the key geological unit, which
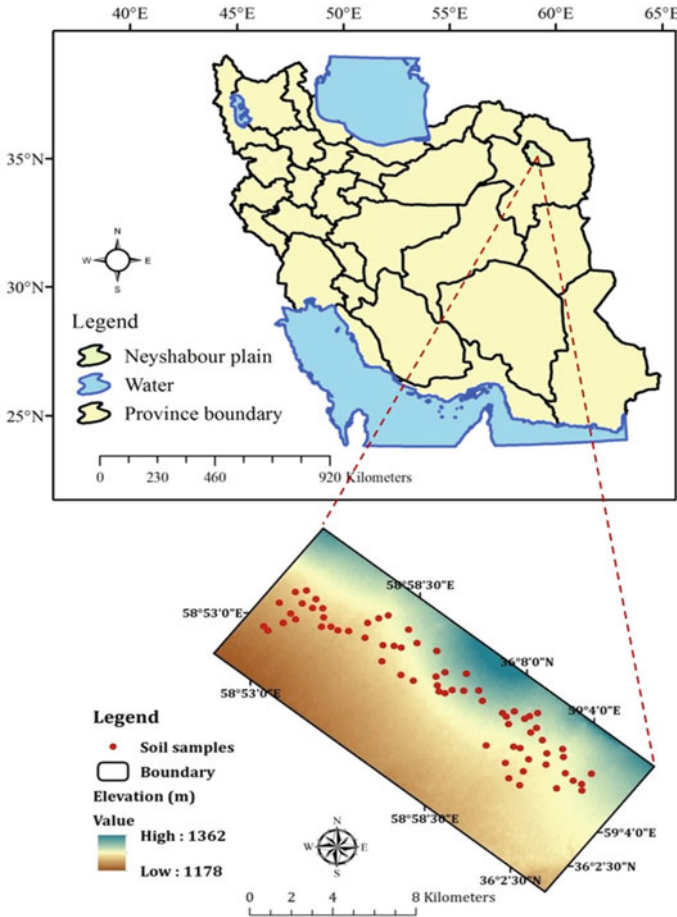
Fig. 12.1 Soil sampling locations in parts of Neyshabur Plain, Khorasan-e-Razavi region, Iran

indicates low levels of piedmont fan and valley terrace deposits. Aridisols and Entisols are the most common soil types in the area, according to Bagherzadeh et al. (2016).

12.3 Methods

12.3.1 Sampling and Analysis

Sixty-eight representative soil samples (during the period between 2018 and 2019) were collected using a random sampling technique for an suitable demarcation of soil

sampling areas to reflect the geographical distribution of the parameters distressing the soils and heavy metals. A portable Global Positioning System (GPS) was applied during soil sampling to find the sampling locations. Soil samples were taken from 0 to 20 cm because our goal was to focus on the topsoil, or the part of the soil influenced by crop roots and water infiltration. Large plant materials and pebbles in the samples were parted by hand and discarded. Bulk samples of the soil were spread on trays in the laboratory and were air-dried for two weeks under ambient conditions. The samples were subsequently tiled in a 2 mm mesh and dried in an oven at 50 °C for approximately 48 h with mortar and pestle (Lu et al. 2010). The samples were then homogenated and placed in polyethylene containers. The hydrometer method was used to determine the textural fractions of sand (0.05–2 mm), silt (0.002–0.05 mm), and clay (<0.002 mm) in soil (Gee and Bauder 1986). The approach of Walkley and Black was used to quantify the number of organic carbon (OC) in the soil (Walkley and Black 1934). The method of Olsen et al. (1954) was used to determine the amount of available phosphorus (P). The process of extraction with 1 M ammonium acetate (NH_4OAC) at pH = 7 was used to quantify available potassium (K) (Thomas 1996). A digital EC-pH metre was used to measure pH in saturated paste extract (Thomas 1996). An atomic absorption spectrometer was used to analyse heavy metals like Mn, Fe, Zn, and Cu. Following the procedure of Heidari et al. (2019) the soil samples were digested using the aqua-regia process (HNO_3:HCl in a ratio of 1:3). The digested samples were filtered and diluted in 20 mL double steam distilled water before being utilised in the experiment. After every five samples, the standards and blanks were run for quality assurance and quality control to ensure the machine's 95% accuracy (Arora et al. 2008). The 95–100% recovery rates for samples spiked with standards confirmed the accuracy of the results (Xiao et al. 2013).

12.3.2   Statistical Analysis

The use of statistical methods helps us understand the dynamic soil quality data matrices, classify potential causes that affect soil resources, and provide useful knowledge for effective soil management (Simeonov et al. 2004; Reghunath et al. 2002). The correlation matrix was performed using Microsoft Excel version 2013. *Pearson's* correlation was done by the correlation matrix of soil heavy metal parameters. A correlation coefficient (near +1 or −1) means that a strong relationship between two variables is established and '*0*' indicates that no relationship occurs between them. All the statistical analyses were performed at a significance level of $P < 0.05$.

12.3.2.1   Incremental Spatial Autocorrelation

The Incremental Spatial Autocorrelation (ISA) method uses the *Global Moran's I* function, which calculates the strength of spatial clustering for each of the distances,

to construct a sequence of that distances, and can be intended based on the following equation:

$$I = \frac{n}{S_0} \frac{\sum_{i=1}^{n} \sum_{j=1}^{n} \omega_{i,j}, Z_i Z_j}{\sum_{i=1}^{n} Z_i^2}$$

where, Z_i is the deviation of heavy metallic soil parameters for sample location i from its mean $(x_i - \overline{x})$, $\omega_{i,j}$ is the spatial weight between sample location i and j, n is equal to the total number of sampling sites, S_0 is the cumulative of all the spatial weights:

$$S_0 = \sum_{i=1}^{n} \sum_{j=1}^{n} w_{i,j}$$

The *Moran 's Index* is positive because the data collection continues to cluster geographicalluy (high values cluster next to other high values, low values cluster near other small ones). The index would be negative if high values repel certain interests and appear to be close to low. If positive cross-product values surpass negative cross-product values, the index will be close to zero. The numerator is determined by the variation in order to minimize index values from -1.0 to $+1.0$.

The ISA mechanism can be the extent to which high (clustered) or low (dispersed) spatial correlations and whether they have been significant or not detected by a peak suggested by the index. This can be both measures of distance are based on the feature centers, and the default start distance (500 m) is the smallest distance (each feature has at least one nearby area). The clustering strength is determined by the returned z-point. Typically, the z-score, indicating an increasing clustering, increases as the gap increases. The z-score usually peaks at a certain point (Jossart et al. 2020). However, when there is more than one statistically significant peak, the clustering at each of these distances is pronounced. Select the maximum distance that best fits the size of the study you want; it is also the first statistically relevant summit that has been identified.

12.3.2.2 Optimized Cluster Analysis

The mapping tools perform cluster analysis in order to determine the location of hotspots, coldspots, spatial outliers, and similar features or areas of statistically significant importanceusing the *Anselin Local Moran's I* statistic (Anselin 1995). The tool is particularly useful for intervention dependent on the location of one or more clusters. This method distinguishes statistically important spatial clusters with high (hot) and low (cold) values. The system aggregates heavy metallic soil data automatically, determines the appropriate analysis scale, and corrects multiple tests as well as spatial dependency.

Since the *Optimized Outlier Analysis* tool uses the nearest average and median next-door calculations for aggregation and also for an adequate scale of analysis, a component for initial data assessment will also identify locations in each soil characteristics at geographical locations. This method measures the average closest distance of each element and compares all the distances spread.

12.3.2.3   Estimation of Spatial Interpolation of Soil Parameters

Spatial patterns, values in unmeasured areas, and the uncertainty associated with a predicted value in unmeasured locations may be determined by Kernal Smoothing (KS). KS is used to model and measure the spatial variability in the sampled places of each of the influential parameters (Gribov and Krivoruchko 2004). The Z vector p() theory is based on both randomly and spatially autocorrelated. The predictions are model-based on:

$$Z(p_i) = \mu + \varepsilon'(p_i)$$

where μ is the constant stationary function (global mean) and $\varepsilon'(p_i)$ is the spatially correlated stochastic part of the variation. The forecasts are collected with:

$$\hat{Z}_{ok}(p_0) = \sum_{i=1}^{n} w_i(p_0) \cdot Z(p_i) = \lambda_0^T \cdot a$$

where λ_0 is the vector of kriging weights (w_i), a is the vector of n observations at primary locations.

The semivariogram is a convenient tool for analyzing spatial dependence structures in geostatistics. It is focused on the basic difference and is defined by:

$$\gamma(h) = \frac{1}{2} Var(Z(p_i) - Z(p_i + h))^2$$

where $Z(p_i)$ is the value of a random variable at some sampled location and $Z(p_i + h)$ is the value of the location at a distance $(p_i + h)$.

The variogram for each parameter was drawn from a Polynomial, Quartic, Exponential, and Gaussian model, based on the shortest distance between points and determining the best variable model feature. To all kernel functions, r is a radius centered at point s, and h is bandwidth for all formulas (Yan, 2009):

Polynomial $= \left(1 - \left(\frac{r}{h}\right)^3 \left(10 - \left(\frac{r}{h}\right)\left(15 - 6\left(\frac{r}{h}\right)\right)\right)\right), for \frac{r}{h} < 1.$

Quartic $= \left(1 - \left(\frac{r}{h}\right)^2\right)^2, for \frac{r}{h} < 1.$

Exponential $= e^{-3\left(\frac{r}{h}\right)}$.

Gaussian $= e^{-3\left(\frac{r}{h}\right)^2}$.

12.3.2.4 Cross-Validation

For the evaluation and comparison of model performance, a cross-validation technique was adopted. In the model accuracy assessment, the, root mean squared error (RMSE) and average standard error were identified (Zhang et al. 2018).

12.4 Results

12.4.1 *Exploratory Analysis of Soil Variables*

The physico chemical characteristics of soil that eventually affect the root growth and mobility of the contaminant can greatly influence the assimilation of heavy metals. Descriptive statistics of all soil variables are presented in Table 12.1. The soil pH of the research area is ranges between 7.5 and 8.3, with a mean value of 7.9 ± 0.19. The mean value of Organic Carbon (OC), Sand, Silt, clay, Phosphorus (P), Potassium (K), Iron (Fe), Manganese (Mn), Zink (Zn), Copper (Cu) is calculated as 0.73%, 40.29%, 36.99%, 22.72%, 19.45 mg/kg, 261.05 mg/kg, 2.31 mg/kg, 7.18 mg/kg,

Table 12.1 Descriptive characteristics of concentration of heavy metals in soils samples

	Mean	Standard error	Median	Standard deviation	Kurtosis	Skewness	Confidence level (95.0%)
pH	7.90	0.02	7.90	0.19	−0.59	−0.01	0.05
OC (%)	0.73	0.04	0.68	0.32	1.03	1.07	0.08
Sand (%)	40.29	1.18	40.30	9.72	0.34	0.57	2.35
Silt (%)	36.99	0.78	36.90	6.41	−0.53	−0.13	1.55
Clay (%)	22.72	0.73	23.00	5.99	−0.61	−0.26	1.45
Phosphorus (mg/kg)	19.45	1.97	11.20	16.25	0.13	1.09	3.93
Potassium (mg/kg)	261.05	16.16	249.71	133.27	3.10	1.42	32.26
Fe (mg/kg)	2.31	0.08	2.28	0.68	0.20	0.66	0.16
Mn (mg/kg)	7.18	0.49	6.04	4.06	2.53	1.61	0.98
Zn (mg/kg)	2.84	0.46	1.09	3.78	1.58	1.68	0.92
Cu (mg/kg)	1.16	0.04	1.13	0.29	−0.34	0.47	0.07

2.84 mg/kg, 1.16 mg/kg, respectively. The highest standard deviation is calculated for potassium ($\pm$133.27), followed by sand ($\pm$9.72), silt ($\pm$6.41), and clay ($\pm$5.99). The negative kurtosis and skewness are calculated for pH, Silt, Clay, and Cu. The maximum kurtosis is estimated for K (3.10), followed by Mn (2.53) and Zn (1.58). The maximum skewness is calculated for Zn (1.68), followed by Mn (1.61) and K (1.42).

12.4.2   Pearson's Correlation

The correlation coefficient for different soil properties results is presented in Fig. 12.2. The coefficient of correlation between the pH and zinc ($r = 0.41$) has been found to be positive ($P < 0.05$). However non-significant ($P > 0.05$) relationship was found with OC ($r = 0.23$) and Silt ($r = 0.27$). Results also showed strong negative correlation between sand, silt ($r = -0.80$) and clay ($r = -0.77$). There is moderate positive correlation was calculated between sand and zinc; whereas, a negative relationship was found between clay and zinc. Similarly, the meager positive correlation was observed between OC, K, and Mn with available P. A meager negative correlation is observed between available K and zinc, and a positive correlation is calculated with OC. Fe shows a moderate negative correlation with the clay and available K; and a
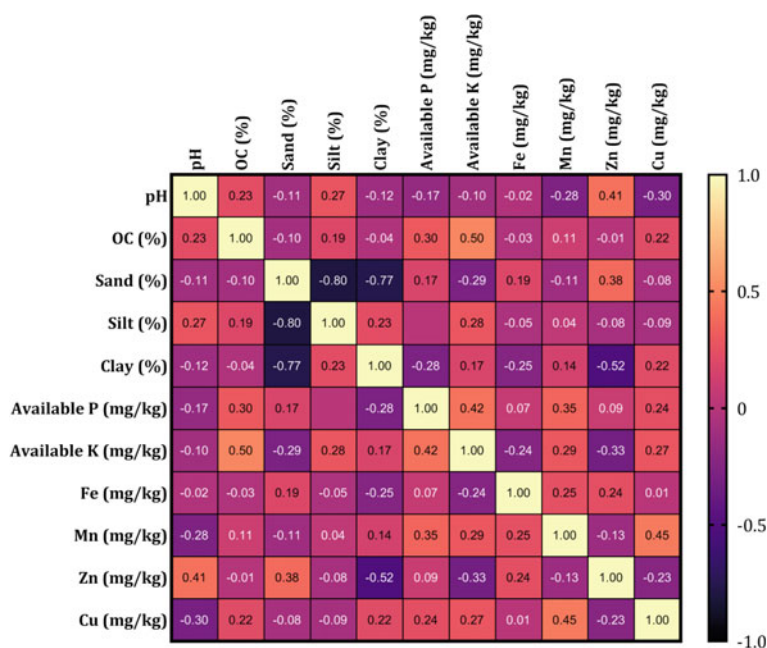

	pH	OC (%)	Sand (%)	Silt (%)	Clay (%)	Available P (mg/kg)	Available K (mg/kg)	Fe (mg/kg)	Mn (mg/kg)	Zn (mg/kg)	Cu (mg/kg)
pH	1.00	0.23	-0.11	0.27	-0.12	-0.17	-0.10	-0.02	-0.28	0.41	-0.30
OC (%)	0.23	1.00	-0.10	0.19	-0.04	0.30	0.50	-0.03	0.11	-0.01	0.22
Sand (%)	-0.11	-0.10	1.00	-0.80	-0.77	0.17	-0.29	0.19	-0.11	0.38	-0.08
Silt (%)	0.27	0.19	-0.80	1.00	0.23		0.28	-0.05	0.04	-0.08	-0.09
Clay (%)	-0.12	-0.04	-0.77	0.23	1.00	-0.28	0.17	-0.25	0.14	-0.52	0.22
Available P (mg/kg)	-0.17	0.30	0.17		-0.28	1.00	0.42	0.07	0.35	0.09	0.24
Available K (mg/kg)	-0.10	0.50	-0.29	0.28	0.17	0.42	1.00	-0.24	0.29	-0.33	0.27
Fe (mg/kg)	-0.02	-0.03	0.19	-0.05	-0.25	0.07	-0.24	1.00	0.25	0.24	0.01
Mn (mg/kg)	-0.28	0.11	-0.11	0.04	0.14	0.35	0.29	0.25	1.00	-0.13	0.45
Zn (mg/kg)	0.41	-0.01	0.38	-0.08	-0.52	0.09	-0.33	0.24	-0.13	1.00	-0.23
Cu (mg/kg)	-0.30	0.22	-0.08	-0.09	0.22	0.24	0.27	0.01	0.45	-0.23	1.00

Fig. 12.2   Cross-correlation matrix of heavy metals in soils samples ($n = 68$)

Table 12.2 Spatial autocorrelation of heavy metals in soils samples

Parameters	Moran's Index	Expected Index	Variance	z-score	P-value
pH	0.749	−0.015	0.041	3.789	0.000
OC (%)	0.392	−0.015	0.040	2.045	0.041
Sand (%)	0.589	−0.015	0.040	3.015	0.003
Silt (%)	0.196	−0.015	0.041	1.047	0.295
Clay (%)	0.820	−0.015	0.041	4.142	0.000
Phosphorus (mg/kg)	0.138	−0.015	0.040	0.762	0.446
Potassium (mg/kg)	−0.041	−0.015	0.038	−0.133	0.894
Fe (mg/kg)	0.360	−0.015	0.040	1.870	0.061
Mn (mg/kg)	0.118	−0.015	0.039	0.677	0.498
Zn (mg/kg)	0.317	−0.015	0.039	1.671	0.095
Cu (mg/kg)	0.298	−0.015	0.040	1.554	0.120

positive correlation with the Mn and Zn. Mn shows a moderate positive correlation with the available P, K, and Fe. Zn shows a moderate positive correlation with the pH, sand, and Fe; whereas, a negative correlation is calculated for clay, available K, and Cu. Statistical outcomes exhibited that Cu, influencedby pH and $CaCO_3$ levels, increased with the moving soil fractions bonding.

The soil pH and the available proportion Cu had a negative association, as per the observations. Based on the bioavailability and chemical processes of heavy metals, binding in various fractions vary considerably. As a result of the apparent competition between dissolved metals, the adsorption of heavy metals has been shown to decrease. Heavy metals on the negative surfaces formed on organic colloidal materials and on minerals, on the other hand, have been documented to adsorb electrostatically (Sungur et al. 2014).

Table 12.2 shows the spatial autocorrelation of heavy metals of soil samples in the part of Neyshabur plain of Khorasan-e-Razavi Province. The significance of Moran's I is tested ($P < 0.05$). The maximum *Moran's I* is calculated for clay (8.20), followed by pH (0.749) and sand (0.589), and the corresponding *P-values* are calculated as <0.0001. It represents a significant positive correlation between the sample values and is clustered pattern. Moreover, the calculated value of Moran's *I* of silt, P, Mn, K are very close to zero, and the corresponding Z-score and *P-values* are not significant. This indicates a uniform distribution pattern of soil heavy metal contents (silt, P, Mn, K) in the study area. Zn, Fe, and OC have moderate significant ($P < 0.05$) positive spatial autocorrelation among sample values in the study area.

12.4.3   Spatial Autocorrelation

The statistical existence of data sets based on the distance between high auto-correlation in the spatial area is taken into consideration. It typically can be accomplished through an iterative and data-led process that determines how spatial auto-correlation occurs differs at various distances. For each increase in distance, space autocorrelation measures the associated *Moran's I*, Expected Index, Variance, z-score, and p-values for a number of distance increments and reports. High Z-scores value suggested statistical significance ($P < 0.05$). This means that heavy metal concentrations are higher in Z-score based upon allocations of spatial variability and metal heterogeneity at different soil depths (Ren et al. 2016). The threshold value of the beginning distance is considered as 500 m, and the incremental threshold distance specified as 1030, 1560, 2091, 2621, 3152, 3682, 4213, 4743, and 5274 m (Table 12.3). The high value of *Moran's I* indicate the distance at which the clustering of the data is more affirmed. The highest *Moran's I* value at 500 m is calculated for pH (Z-score—3.065; *P*-value <0.002) and clay (Z-score—3.496; *P*-value <0.000), followed by Sand (Z-score—2.218; *P*-value <0.033) and OC (Z-score—2.316; *P*-value <0.020). At 1030 m distance, the maximum *ISA* is calculated for clay (*Moran's I*—0.664; Z-score—6.891; *P*-value <0.000), followed by Zn (*Moran's I*—0.424; Z-score—4.547; *P*-value <0.000) and F (*Moran's I*—0.403; Z-score—4.277; *P*-value <0.000). At a distance of 1560 m, maximum ISA is calculated for clay (*Moran's I*—0.597; Z-score—9.492; *P*-value <0.000), followed by Zn (*Moran's I*—0.475; Z-score—7.717; *P*-value <0.000) and pH (*Moran's I*—0.372; Z-score—6.002; *P*-value <0.000). However, the derived output of ISA value for clay and Zn is maximum at each threshold distance. Moreover, the minimum estimated ISA value is calculated for P and Mn at each distance band at which the sample locations are uniformly distributed.

12.4.4   Cluster Analysis

The GiZ-Score map is generated by the optimal cluster analysis (OCA) tool, which shows the hot and cold locations in the study area. It also provides point features in the research region that signify hot and cold locations (Fig. 12.3). GiZScore is a tool that creates a z-score value for each sampling location, which serves to identify the statistical significance of feature clusters and, ultimately, hot and cold locations. Heavy metallic parameters of soil characteristics with a high positive z-score are designated as hotspots (red), while heavy metallic elements of soil features with a low z-score are designated as cold spots (blue). The z-score is used to determine whether the sampling location exhibit a random pattern or statistically significant clustering or dispersion, indicating a spatial process at work. As a result, the greater the value for a statistically significant positive z-score, the more intense the clustering of the hotspot.

Table 12.3 Incremental spatial autocorrelation analysis of heavy metals in soils samples

Distance (m)	500			1030			1560			2091			2621		
Soil parameter	Moran's index	z-score	p-value	Moran's index	z-score	p-value	Moran's index	z-score	p-value	Moran's index	z-score	p-value	Moran's index	z-score	p-value
pH	0.607	3.065	0.002	0.393	4.139	0.000	0.372	6.002	0.000	0.264	5.824	0.000	0.246	6.474	0.000
OC (%)	0.401	2.128	0.033	0.012	0.286	0.775	0.054	1.090	0.276	0.019	0.722	0.470	0.013	0.691	0.489
Sand (%)	0.446	2.316	0.020	0.307	3.292	0.001	0.289	4.747	0.000	0.205	4.625	0.000	0.176	4.785	0.000
Silt (%)	0.218	1.190	0.233	−0.064	−0.496	0.620	−0.012	0.044	0.965	−0.015	0.008	0.993	−0.016	−0.021	0.983
Clay (%)	0.696	3.496	0.000	0.664	6.891	0.000	0.597	9.492	0.000	0.526	11.290	0.000	0.469	12.035	0.000
Phosphorus (mg/kg)	0.227	1.288	0.197	0.275	2.973	0.003	0.054	1.087	0.277	0.000	0.313	0.754	−0.038	−0.583	0.559
Potassium (mg/kg)	−0.015	0.065	0.948	0.038	0.563	0.573	0.092	1.711	0.087	0.051	1.422	0.155	0.056	1.798	0.072
Fe (mg/kg)	0.400	2.092	0.036	0.403	4.277	0.000	0.352	5.725	0.000	0.235	5.256	0.000	0.248	6.581	0.000
Mn (mg/kg)	0.184	1.094	0.274	0.163	1.854	0.063	0.156	2.707	0.006	0.142	3.347	0.000	0.130	3.691	0.000
Zn (mg/kg)	0.266	1.451	0.146	0.424	4.547	0.000	0.475	7.717	0.000	0.440	9.641	0.000	0.429	11.225	0.000
Cu (mg/kg)	0.312	1.676	0.094	0.234	2.538	0.011	0.167	2.828	0.004	0.172	3.924	0.000	0.160	4.361	0.000

Distance (m)	3152			3682			4213			4743			5274		
Soil parameter	Moran's index	z-score	p-value	Moran's index	z-score	p-value	Moran's index	z-score	p-value	Moran's index	z-score	p-value	Moran's index	z-score	p-value
pH	0.216	6.664	0.000	0.178	6.302	0.000	0.154	6.123	0.000	0.143	6.203	0.000	0.132	6.289	0.000
OC (%)	0.005	0.582	0.558	0.031	1.533	0.125	0.032	1.706	0.088	0.016	1.264	0.205	−0.021	−0.249	0.802

(continued)

Table 12.3 (continued)

| Distance (m)	3152			3682			4213			4743			5274		
Soil parameter	Moran's index	z-score	p-value	Moran's index	z-score	p-value	Moran's index	z-score	p-value	Moran's index	z-score	p-value	Moran's index	z-score	p-value
Sand (%)	0.158	5.036	0.000	0.137	5.002	0.000	0.132	5.349	0.000	0.082	3.833	0.000	0.038	2.298	0.022
Silt (%)	−0.015	−0.021	0.982	−0.016	−0.022	0.983	0.008	0.821	0.411	−0.017	−0.086	0.931	−0.025	−0.437	0.662
Clay (%)	0.420	12.570	0.000	0.362	12.302	0.000	0.326	12.310	0.000	0.268	11.152	0.000	0.204	9.360	0.000
Phosphorus (mg/kg)	−0.037	−0.652	0.514	−0.031	−0.543	0.587	−0.035	−0.741	0.459	−0.042	−1.059	0.289	−0.028	−0.577	0.564
Potassium (mg/kg)	0.090	3.123	0.002	0.102	3.920	0.000	0.094	4.058	0.000	0.076	3.717	0.000	0.059	3.273	0.001
Fe (mg/kg)	0.185	5.817	0.000	0.135	4.908	0.000	0.095	3.999	0.000	0.070	3.390	0.000	0.043	2.489	0.012
Mn (mg/kg)	0.101	3.429	0.000	0.099	3.809	0.000	0.073	3.281	0.001	0.072	3.536	0.000	0.061	3.350	0.000
Zn (mg/kg)	0.404	12.331	0.000	0.350	12.101	0.000	0.308	11.861	0.000	0.259	10.950	0.000	0.206	9.595	0.000
Cu (mg/kg)	0.119	3.903	0.000	0.082	3.139	0.001	0.047	1.733	0.082	0.029	1.733	0.082	0.016	1.343	0.017
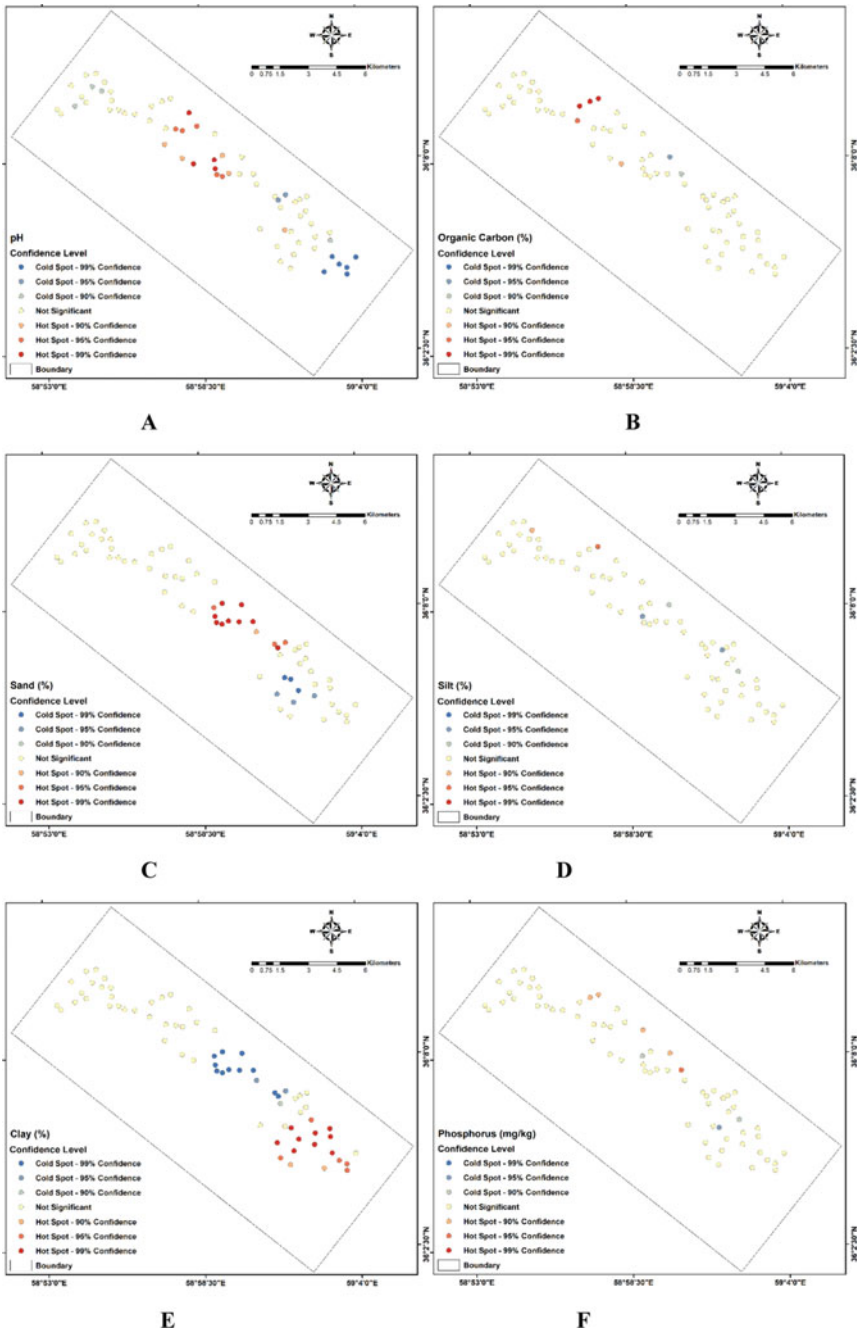
Fig. 12.3 Optimized cluster analysis of soil samples using Getis-Ord Gi* statistics
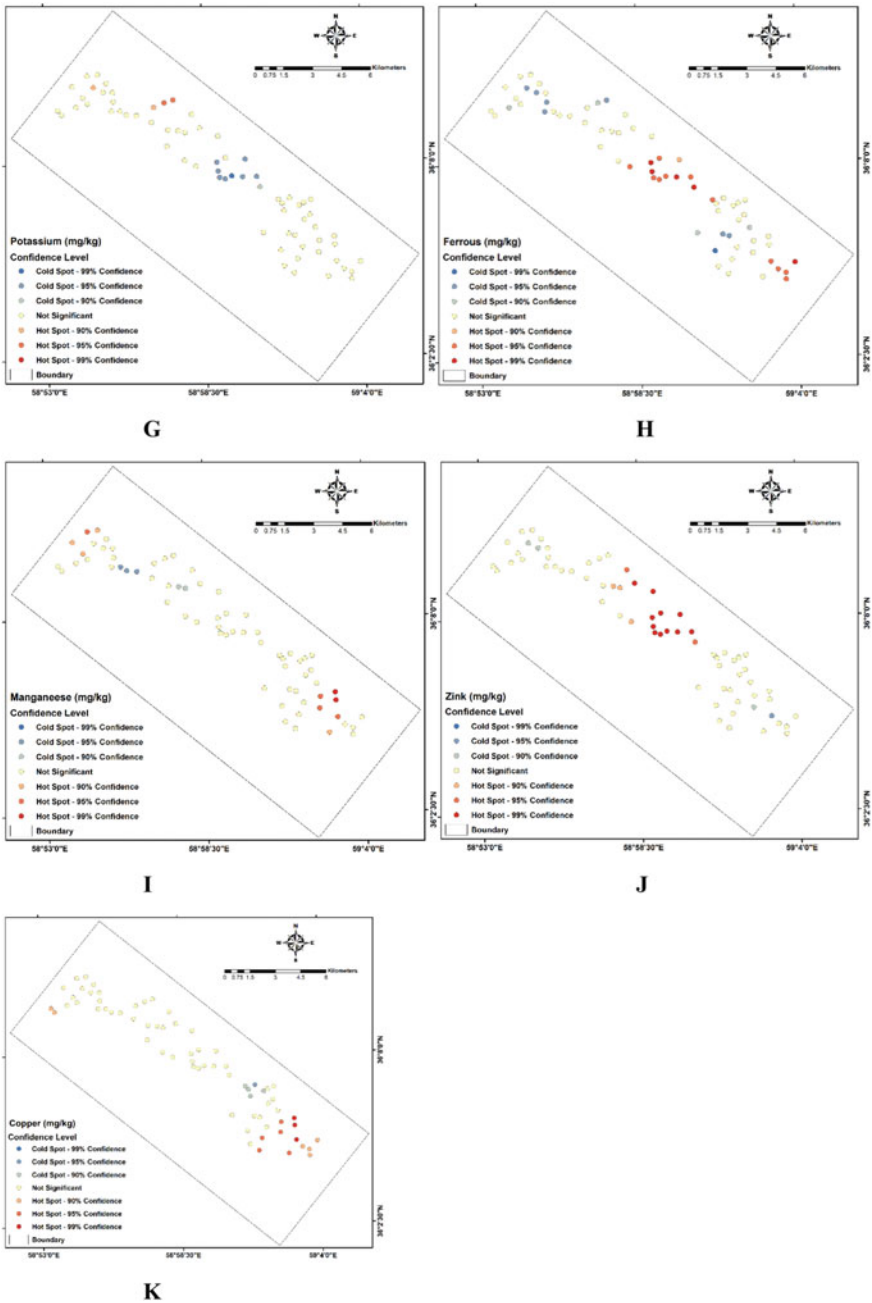
G

H

I

J

K

Fig. 12.3 (continued)

In Fig. 12.3a, it can be seen that hotspots and coldspots are presented by pH where the values were $2.946422 > z > 1.767853$ (red) and $-3.17487 < z < -1.785019$ (blue) standard deviations, respectively. The hotspots and coldspots of OC are presented as $3.101711 > z > 1.952999$ (red) and $-2.117656 < z < -1.714938$ (blue) standard deviations, respectively (Fig. 12.3b). The significance of hotspots and coldspots of sand are presented as $4.249433 > z > 2.203002$ (red) and $-3.046544 < z < -2.02786$ (blue) standard deviations, respectively (Fig. 12.3c). The standard deviations of the hotspots and coldspots of Silt are $2.1069 > z > 1.793934$ (red) and $-2.514968 < z < -1.886327$ (blue) (Fig. 12.3d). The significance of hotspots and coldspots of clay are presented as $3.736432 > z > 1.858045$ (red) and $-4.870407 < z < -2.229149$ (blue) standard deviations, respectively (Fig. 12.3e). Hotspot and cold spot as indicated by P, with standard deviations of $2.263199 > z > 1.767853$ (red) to $-2.233934 < z < -1.848018$ (blue) (Fig. 12.3f). K showing $2.266854 > z > 1.797812$ and $-2.688332 < z < -1.710025$ (blue) standard deviations are the hotspots and coldspots (Fig. 12.3g). The hotspots and coldspots are presented by Fe, where the values were $2.959069 > z > 1.846312$ (red) and $-2.60816 < z < -1.876887$ (blue) standard deviations, respectively (Fig. 12.3h). Mn shows the hotspots and cold spots with standard deviations of $3.227574 > z > 1.757108$ (red) and $-2.232847 < z < -1.700522$ (blue) (Fig. 12.3i). Zn displays hotspots and coldspots with $4.940435 > z > 1.759745$ (red), and $-1.968598 < z < -1.817021$ (blue), respectively, standard deviations (Fig. 12.3j). Coldspots and hotspots are presented with the values of Cu with standard deviations of $2.977647 > z > 1.917672$ (red) and $-2.112617 < z < -1.763338$ (blue) (Fig. 12.3k).

12.4.5   Spatial Distribution

The aim is to test the performance in heavy metal parameters, combination with estimation and simulation, of four different semivariogram models to explain their uncertainty and spatial heterogeneity. In Table 12.4, along with their respective best-fit results, the simulated semivariogram for the Polynomial, Quartic, Exponential, and Gaussian models is evaluated in order to illustrate the spatial dependence of heavy metal accumulation in soil. The exponential and gaussian models looked similar except for the slight difference in soil heavy metals distribution patches.

In order to map the metal content and delineate the polluted areas, a spatial correlation between the data available with the kernel smoothing technique was used. The results showed that the exponential model was well-matched with the soil heavy metal data (Fig. 12.4). The highest value of pH is observed in the central part and a small pocket north of the study area. The low pH value is observed in the south and east of the region. The pH value of 7.95–8.1 is also observed in the middle of the study area. The maximum concentration of OC is found in the central and northwest of the study area. The medium concentration of OC is portrayed in the central and eastern parts of the study area. The minimum concentration of OC is found in the west and south of the region. The maximum concentration of sand is observed in the

Table 12.4 Best-fitted models used for soil characteristics

Soil samples	Model	Mean	RMSE	Avg. SE
pH	Polynomial5	−0.011	0.159	0.425
	Quartic	−0.011	0.161	0.423
	Gaussian	−0.014	0.160	0.433
	Exponential	−0.013	0.158	0.427
Organic Carbon (%)	Polynomial5	0.111	0.365	0.315
	Quartic	0.112	0.363	0.313
	Gaussian	0.112	0.363	0.307
	Exponential	0.109	0.358	0.312
Sand (%)	Polynomial	1.888	9.312	55.05
	Quartic	1.918	9.27	55.03
	Gaussian	1.972	9.23	54.9
	Exponential	1.888	9.118	54.11
Silt (%)	Polynomial5	0.804	7.076	39.031
	Quartic	0.782	6.985	38.755
	Gaussian	0.780	6.851	38.426
	Exponential	0.745	6.896	38.269
Clay (%)	Polynomial5	0.301	4.192	18.064
	Quartic	0.286	4.185	18.049
	Gaussian	0.260	4.192	18.072
	Exponential	0.243	4.088	17.71
Phosphorus (mg/kg)	Polynomial5	8.863	18.597	59.975
	Quartic	8.991	18.44	60.105
	Gaussian	9.986	18.685	61.16
	Exponential	8.518	18.339	61.201
Potassium (mg/kg)	Polynomial5	55.869	174.706	2361.018
	Quartic	57.395	172.825	2352.581
	Gaussian	60.023	166.594	2339.885
	Exponential	55.860	174.14	2308.157
Fe (mg/kg)	Polynomial5	0.068	0.553	0.819
	Quartic	0.068	0.552	0.825
	Gaussian	0.072	0.544	0.841
	Exponential	0.067	0.555	0.828
Mn (mg/kg)	Polynomial5	1.503	4.346	12.266
	Quartic	1.554	4.496	11.764
	Gaussian	1.869	4.579	12.593
	Exponential	1.365	4.433	12.214

(continued)

Table 12.4 (continued)

Soil samples	Model	Mean	RMSE	Avg. SE
Zn (mg/kg)	Polynomial5	1.452	3.519	5.384
	Quartic	1.462	3.521	5.456
	Gaussian	1.566	3.529	5.589
	Exponential	1.421	3.516	5.421
Cu (mg/kg)	Polynomial5	0.053	0.277	0.292
	Quartic	0.053	0.277	0.292
	Gaussian	0.060	0.281	0.295
	Exponential	0.049	0.274	0.291

northcenter of the study area. However, the minimum sand concentration is observed south and northwest of the study area. The spatial distribution of silt is varied in the study area, whereas the maximum sand distribution is found in the south-center and northwest and its gradually decreases from the central region. There is a heterogeneous distribution of Zn concentration in the study area. Fe is heterogeneously distributed in the study area. The maximum Mn is portrayed in the north and east of the region, andtheminimum Mn is observed in the central and west of the region. The highest Fe is found in the central and east of the study site, and the south and west part is recorded as low Fe concentration. The maximum concentration of Zn is found in the east and west of the study area whereas, the central part of the region is recorded as low concentration of Zn. The highest concentration of Cu is observed in the east and central north of the region and south of the study area with low Cu concentration.

12.5   Discussion

In several regions of the world, particularly in developing countries, metal soil pollution has become a major and pervasive challenge. Farming may be a source of heavy metals in the soil (Huang and Jin 2008), urbanization, industrial development, andmining (Zhong et al. 2012). Heavy metal pollution is mainly due to urban and industrial aerosols, burning of fuel, liquid and solids, mining waste, industrial and farm chemicals, etc. The soils are primarily drained by different soil areas where either the inorganic or organic colloids are preserved very strongly. The weathering of the parents' materials means that heavy metals are existing in all uncontaminated soils. Chemical waste inorganic contaminants cause serious waste disposal issues. Superphosphate, phosphoric acid, aluminum, steel, and ceramics industry fluorides can be found in the atmosphere. 55.89% of the total samples haveapH value >7.90. Most trace elements' solubility decreases when soil pH rises, resulting in low quantities in soil solution (Kabata-Pendias 2011). Any change in the pH of the soil has
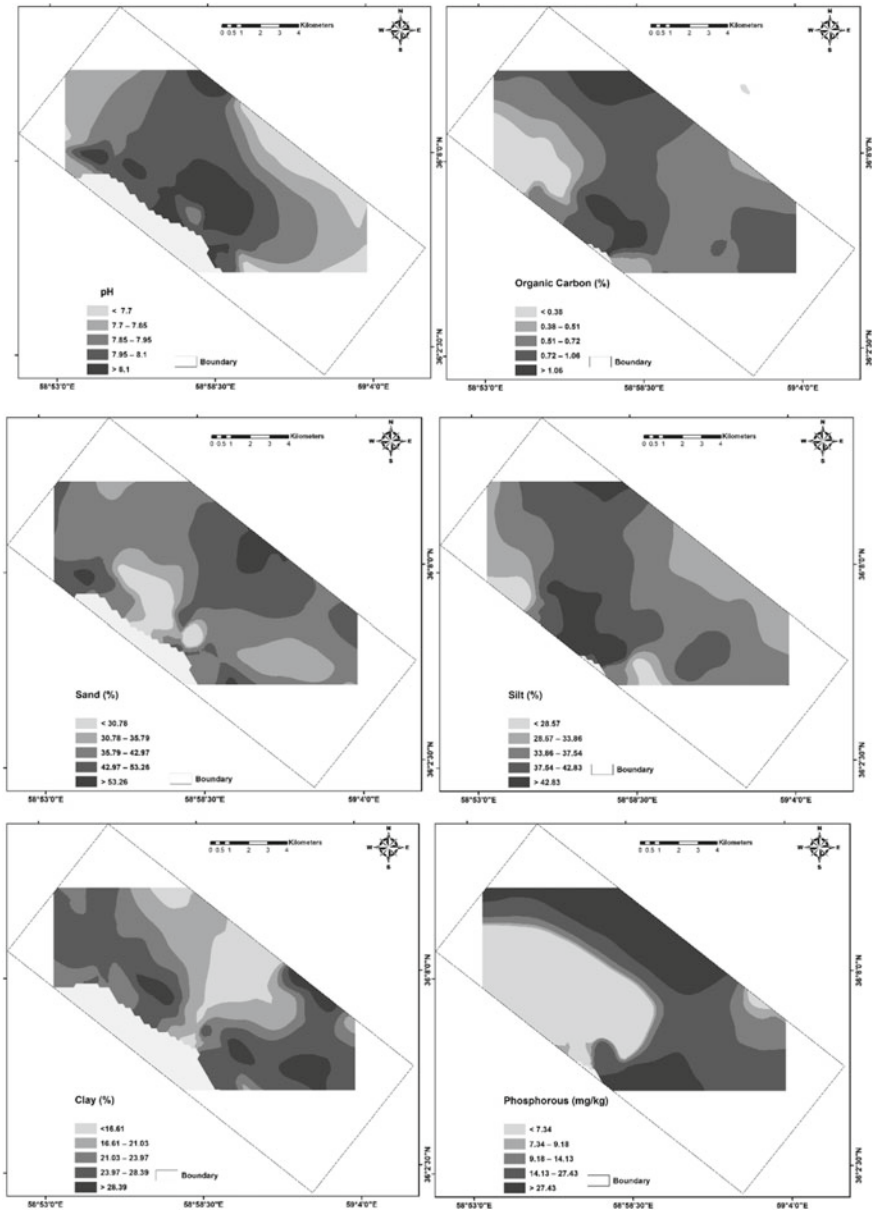
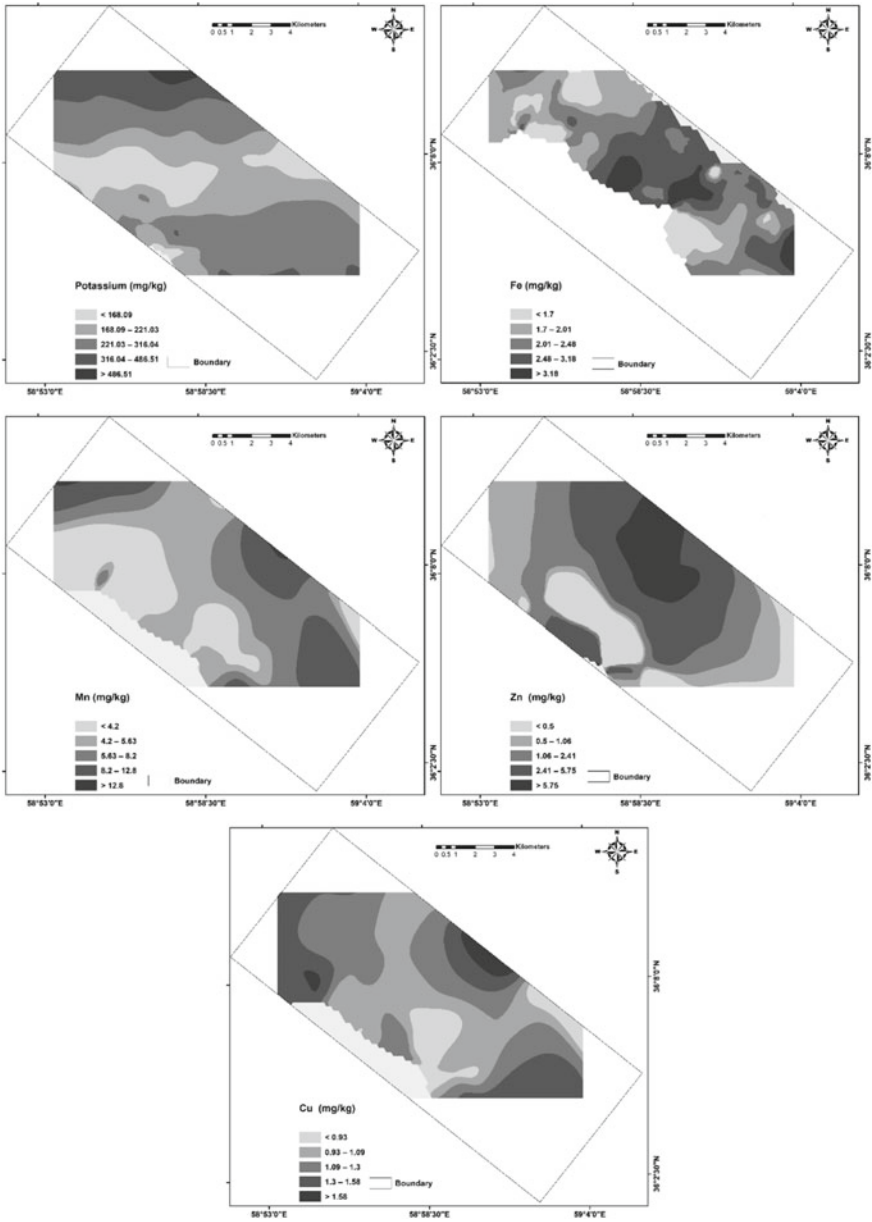**Fig. 12.4** Spatial variability maps of physico-chemical parameters and heavy metals

Fig. 12.4 (continued)

an impact on the solubility of metals. This is likely to be dependent on the metals' ionic species and the pH change's direction. 42.65% P concentration is significantly increased (>16 mg/kg) from the topsoil to the subsoil, indicating that the subsoil aced as sink or source for P leaching. As a result, subsurface products may be evaluated for the implementation of mitigation measures to prevent P leaching in soil horizons based on the P content and the soil saturation threshold (Andersson et al. 2015). Soils can be very acidic by sulfur dioxide emitted by plants and thermal plants. These metals damage the leaf and destroy plant life (Richardson et al. 2006). Water irrigation with sewage is responsible for deep irrigation vicissitudes in the soils. Numerous variations in the soil as an offset of sewage irrigation comprise physical changes such as leaching, humus deviations, porosity, etc., and chemical changes such as soil reactions, soil base exchanges, salinity, nutrient quantities, and nutrient accessibility nitrogen, potash, phosphorus and so forth. This can result in plant phytotoxicity.

Metal ions reach the water of the soil at various such concentrations by which they may either stay in the water or reach drainages to be consumed by plants increasing on the soil or be preserved in sparingly soluble or insoluble soil types (Urzelai et al. 2000). This soil's organic matter is very similar to heavy metal cations, which form stable complexes and thus reduce its nutrient content. However, one or two of the elements in agricultural soils can be concentrated in several ways, such as chemicals, sewage sludge, farm slurries, etc. Increased doses of fertilizer, pesticides, or agricultural chemicals are added over a period of time to contaminate soils using heavy metals. There are also cadmium residuesin some phosphatic fertilizers that can be found in these soil areas. Soil micronutrient accessibility measures parent materials, the effects of soil redox potentials, pH, soil microbial activity, interactions with coexisting ions, soil mineral reactions, and organic matter, as well as the effects of soil edaphic and biological factors activity in the study area. Pearson's correlation coefficient analyzed the relationship between different physico-chemical properties and heavy metal values. A bivariant approach is used for defining the interaction between two different parameters. Agricultural practices, including soil water control application and soil modifications, will make soil micronutrients available. Crop residues are a major source of many micronutrients. Roughly 50–80% of the rice and wheat crops used in Zn, Cu, and Mn may be recovered by incorporating residues (Dhaliwal et al. 2019).

In order to transform test point data on sampling sites into thematic maps showing the geographical variation, traditional interpolator processes like the Generalized Kriging method, a polynomial method, and the Inverse Distance Weighting (IDW) approaches were widely used (Rodrigo-Comino et al. 2019). In comparison, the variogram model is used by the Kriging interpolation method to illustrate the structure of the geographical change of assessed values and the spatial autocorrelation in the modeling of the surface (Wang et al. 2017). The kriging technique includes a collection of methods of stochastic-based interpolation, such as ordinary kriging, cokriging, universal kriging, simple kriging, residual methods, and regression methods (Li and Heap 2014).

Soils of low Zn may have low total Zn (some acidic leached soils in the tropical world) or may have a relatively high total Zn content; however, because of the soil chemistry, a plant-accessible fraction that favors the synthesis of poorly soluble Zn complexes (Rengel 2002). Intensive cultivation of high yield rice and wheat threatened the continued high levels of food production with a Zn and Fe shortfall in rice and Mn weight of wheat. It is widely known to be one of the most operative procedures of growing OC levels and improving soil quality in the application of organic materials. A significant cultivation activity in terms of crop yield and efficiency, climate conservation, and soil regeneration is the use of appropriate quantities of fertilizer (Oenema et al. 2009; Atafar et al. 2010). As a guideline, 15 kg of both phosphorus and sulfur are available to plants for every ton of carbon in OC as organic matter is demolished (Hoyle et al. 2013). As a result, locations with a lot of heavy metal would pollute the soil and put people's and other living organisms' health at risk. The soil concentrations of these metals were higher than critical concentrations in the majority of the field, but their presence in the soil reduces solubility and bioavailability (Krami et al. 2013). The low metal contamination levels in other parts of the region indicate that those areas are safe regions.

12.6 Conclusion

In the present study, geostatistical techniques, correlation matrix, spatial autocorrelation, and spatial modeling were used to analyze the geographical distribution pattern and concentration of heavy metals in Neyshabur plain region in Iran. The outcomes of the geostatistical techniques have confirmed the gravity of pollution and their anthropogenic impact based on spatial changes in contamination levels. The genesis of the pollution process was influenced by natural factors (e.g., the high soil shale, the sandstone, the calcareous and the metamorphic parents and the background values) as well as by anthropogenic factors (e.g., waste disposal, extraction from mines of special mineral ores and high, unmanaged uses of fertilizer). Although nearly all the monitoring classes of land use suffered from contamination by heavy metals, farmland was the most polluted. This information will help land use planners and environmental risk administrators.

Disclosure Statement No potential conflict of interest was reported by the author(s).

References

Andersson H, Bergström L, Ulén B, Djodjic F, Kirchmann H (2015) The role of subsoil as a source or sink forphosphorus leaching. J Environ Qual 44:535–544

Anselin L (1995) Local indicators of spatial association-LISA. Geogr Anal 27(2):93–115

Atafar Z, Mesdaghinia AR, Nouri J, Homaee M, Yunesian M, Ahmadimoghaddam M, Mahvi AH (2010) Effect of fertilizer application on soil heavy metal concentration. Environ Monit Assess 160(1–4):83–89

Bagherzadeh A, Ghadiri E, Darban ARS, Gholizadeh A (2016) Land suitability modeling by parametric-based neural networks and fuzzy methods for soybean production in a semi-arid region. Model Earth Syst Environ 2(2):104

Bhattacharya A, Routh J, Jacks G, Bhattacharya P, Mörth M (2006) Environmental assessment of abandoned mine tailings in Adak, Västerbotten district (northern Sweden). Appl Geochem 21:1760–1780

Dhaliwal SS, Naresh RK, Mandal A, Singh R, Dhaliwal MK (2019) Dynamics and transformations of micronutrients in agricultural soils as influenced by organic matter build-up: a review. Environ Sustain Indicators 1–2:100007

Doabi SA, Karami M, Afyuni M, Yeganeh M (2018) Pollution and health risk assessment of heavy metals in agricultural soil, atmospheric dust and major food crops in Kermanshah province, Iran. Ecotoxicol Environ Saf 163:153–164

Doabi S, Karami M, Afyuni M (2019) Heavy metal pollution assessment in agricultural soils of Kermanshah province, Iran. Environ Earth Sci 78:70

Gee GW, Bauder JW (1986) Methods of soil analysis: part 1. Agronomy handbook 9. In: Klute A (ed) Particle size analysis. American Society of Agronomy and Soil Science Society of America, Madison (WI), pp 383–411

Gribov A, Krivoruchko K (2004) Geostatistical mapping with continuous moving neighbourhood. Math Geol 36(2)

Heidari A, Kumar V, Keshavarzi A (2019) Appraisal of metallic pollution and ecological risks in agricultural soils of Alborz province, Iran, employing contamination indices and multivariate statistical analyses. Int J Environ Health Res 1–19

Hou D, O'Connor D, Nathanail P, Tian L, Ma Y (2017) Integrated GIS and multivariate statistical analysis for regional scale assessment of heavy metal soil contamination: a critical review. Environ Pollut 231:1188–1200

Hoyle FC, Antuono MD, Overheu T, Murphy DV (2013) Capacity for increasing soil organic carbon stocks in dryland agricultural systems. Soil Res 51:657–667

Huang S-W, Jin J-Y (2008) Status of heavy metals in agricultural soils as affected by different patterns of land use. Environ Monit Assess 139(1–3):317–327. https://doi.org/10.1007/s10661-007-9838-4

Jossart J, Theuerkauf SJ, Wickliffe LC, Morris Jr. JA (2020) Applications of spatial autocorrelation analyses for marine aquaculture siting. Front Mar Sci. https://doi.org/10.3389/fmars.2019.00806

Kabata-Pendias A (2011) Trace elements in soils and plants. CRC Press, Boca Raton, FL, USA

Khamesi A, Khademi H, Zeraatpisheh M (2020) Biomagnetic monitoring of atmospheric heavy metal pollution using pine needles: the case study of Isfahan, Iran. Environ Sci Pollut Res 27:31555–31566. https://doi.org/10.1007/s11356-020-09247-5

Krami LK, Amiri F, Sefiyanian A, Shariff AR, Tabatabaie T, Pradhan B (2013) Spatial patterns of heavy metals in soil under different geological structures and land uses for assessing metal enrichments. Environ Monit Assess 185(12):9871–9888. https://doi.org/10.1007/s10661-013-3298-9

Li J, Heap AD (2014) Spatial interpolation methods applied in the environmental sciences: a review. Environ Model Softw 53:173–189

Lu X, Wang L, Li LY, Lei K, Huang L, Kang D (2010) Multivariate statistical analysis of heavy metals in street dust of Baoji, NW China. J Hazard Mater 173:744–749

Moghtaderi T, Mahmoudi S, Shakeri A, Masihabadi MH (2018) Heavy metals contamination and human health risk assessment in soils of an industrial area, Bandar Abbas-South Central Iran. Hum Ecol Risk Assess 24:1058–1073

Moghtaderi T, Mahmodi S, Shakeri A, Masihabadi MH (2019) Contamination evaluation, health and ecological risk index assessment of potential toxic elements in the surface soils (case study: Central Part of Bandar Abbas County). J Soil Water Conserv 8:51–65

Oenema O, Witzke HP, Klimont Z, Lesschen JP, Velthof GL (2009) Integrated assessment of promising measures to decrease nitrogen losses from agriculture in EU-27. Agric Ecosyst Environ 133:280–288

Okrent D (1999) On intergenerational equity and its clash with intragenerational equity and on the need for policies to guide the regulation of disposal of wastes and other activities posing very long time risks. Risk Anal 19:877–901

Olsen SR, Cole CV, Watanabe FS, Dean LA (1954) Estimation of available phosphorus in soils by extraction with sodium bicarbonate. Government Printing Office, Washington. D.C

Parizanganeh A, Hajisoltani P, Zamani A (2010) Assessment of heavy metal pollution in surficial soils surrounding zinc industrial complex in Zanjan-Iran. International society for environmental information sciences 2010 annual conference (ISEIS). Procedia Environ Sci 2:162–166

Ravankhah N, Mirzaei R, Masoum S (2016) Spatial eco-risk assessment of heavy metals in the surface soils of industrial city of Aran-o-Bidgol, Iran. Bull Environ Contam Toxicol 96:516–523

Reghunath R, Murthy TRS, Raghavan BR (2002) The utility of multivariate statistical techniques in hydrogeochemical studies: an example from Karnataka, India. Water Res 36:2437–2442

Ren B, Chen Y, Zhu G, Wang Z, Zheng X (2016) Spatial variability and distribution of the metals in surface runoff in a nonferrous metal mine. J Anal Methods Chem 2016:4515673

Rengel Z (2002) Agronomic approaches to increasing zinc concentration in staple food crops. In: Cakmak I, Welch RM (eds) Impacts of agriculture on human health and nutrition. UNESCO, EOLSS Publishers, Oxford, UK

Richardson GM, Bright DA, Dodd M (2006) Do current standards of practice in Canada measure what is relevant to human exposure at contaminated sites? II: oral bio-accessibility of contaminants in soil. Hum Ecol Risk Assess 12:606–618

Rodrigo-Comino J, Keshavarzi A, Zeraatpisheh M, Gyasi-Agyei Y, Cerdà A (2019) Determining the best ISUM (Improved stock unearthing Method) sampling point number to model long-term soil transport and micro-topographical changes in vineyards. Comput Electron Agric 159:147–156. https://doi.org/10.1016/j.compag.2019.03.007

Santos-Francés F, Martínez-Graña A, Zarza CÁ, Sánchez AG, Rojo PA (2017) Spatial distribution of heavy metals and the environmental quality of soil in the Northern Plateau of Spain by geostatistical methods. Int J Environ Res Public Health 14:568

Simeonov V, Simeonova P, Tzimou-Tsitouridou R (2004) Chemometric quelity assessment of surface waters: two case studies. Chem Eng Ecol 11:449–469

Soffianian A, Bakir HB, Khodakarami L (2015) Evaluation of heavy metals concentration in soil using GIS, RS and geostatistics. IOSR J Environ Sci Toxicol Food Technol 9(12):61–72

Soffianian A, Madani ES, Arabi M (2014) Risk assessment of heavy metal soil pollution through principal components analysis and false color composition in Hamadan Province, Iran. Environ Syst Res 3:3. https://doi.org/10.1186/2193-2697-3-3

Sungur A, Soylak M, Ozcan H (2014) Investigation of heavymetal mobility and availability by the BCR sequential extraction procedure: relationship between soil properties and heavy metals availability. Chem Speciation Bioavail 26(4):219–230. https://doi.org/10.3184/095422914X14147781158674

Thomas GW (1996) Methods of soil analysis: part 2. Agronomy handbook 9. In: Page AL (ed) Soil pH and soil acidity. American Society of Agronomy and Soil Science Society of America, Madison (WI), pp 475–490

Urzelai A, Vega M, Angulo E (2000) Deriving ecological risk-based soil quality values in the Basque Country. Sci Total Environ 247:279–284

Walkley A, Black IA (1934) An examination of the Degtjareff method for determining soil organic matter and a proposed modification of the chromic acid titration method. Soil Sci 37:29–38

Wang G, Zhang S, Xiao L, Zhong Q, Li L, Xu G, Deng O, Pu Y (2017) Heavy metals in soils from a typical industrial area in Sichuan, China: Spatial distribution, source identification, and ecological risk assessment. Environ Sci Pollut Res 24:16618–16630

Xiao R, Bai J, Huang L, Zhang H, Cui B, Liu X (2013) Distribution and pollution, toxicity and risk assessment of heavy metals in sediments from urban and rural rivers of the Pearl River delta in southern China. Ecotoxicology 22(10):1564–1575

Yan X (2009) Linear regression analysis: theory and computing. Published by World Scientific Publishing Co. Pte. Ltd. 5 Toh Tuck Link, Singapore 596224

Zhang LM, Liu YL, Li XD, Huang LB, Yu DS, Shi XZ et al (2018) Effects of soil map scales on simulating soil organic carbon changes of upland soils in eastern China. Geoderma 312:159–169

Zhong L, Liu L, Yang J (2012) Characterization of heavy metal pollution in the paddy soils of Xiangyin County, Dongting lake drainage basin, central south China. Environ Earth Sci. https://doi.org/10.1007/s12665-012-1671-6